U.R.S.I. FRANCE JS 24

Waves for plasma
Plasmas for waves

Theory and simulations of hydrodynamic shocks in a plasma flowing across randomized ICF scale laser beams

Hüller S[1], Ludwig JD[2], Rose HA[3], Bruulsema C[2], Farmer W[2], Michel P[2], Milder A[4], Swadling GF[2], and Rozmus W[4]

[1] *Centre de Physique Théorique CPHT, CNRS, Ecole polytechnique, Insitut Polytechnique Paris, 91128 Palaiseau Cedex, France*
[2] *Lawrence Livermore National Laboratory, 7000 East Avenue, Livermore, California 94551, USA*
[3] *Los Alamos National Laboratory, Los Alamos, New Mexico, USA 87545*
[4] *Department of Physics, University of Alberta, Edmonton, Alberta, Canada T6G 2E1*

Keywords: Laser Shock, laser plasma interaction, Optically smoothed laser beams

Abstract:
High-energy laser beams interacting with flowing plasmas can produce a plasma response that leads to deflection of the beam, beam bending. Such beams have usually a speckle structure generated by optical smoothing techniques that reduce the spatial and temporal coherence in the laser field pattern. The cumulative plasma response from laser speckles slows down the velocity of the incoming flow by momentum conservation. For slightly super-sonic flow the cumulative plasma response to the ponderomotive force exerted by the beam speckle ensemble is the strongest, such that slowing down the flow to subsonic velocities leads eventually to the generation of a shock around the cross section of the beam. This scenario has been predicted theoretically and is confirmed by our hydrodynamic simulations. The conditions of shock generation are given in terms of the ponderomotive pressure, speckle size and the flow velocity. The nonlinear properties of the shocks are analyzed using Rankine-Hugoniot relations. According to linear theory, temporally smoothed laser beams exhibit a higher threshold for shock generation. Numerical simulations with beams that are smoothed by spectral dispersion compare well with the linear theory results, diverging from those produced by beams with only a random phase plates in the nonlinear regime. The conditions necessary for shock generation and their effects on the laser plasma coupling in inertial confinement fusion (ICF) experiments are also discussed.

1 Introduction

The laser facilities designed for Inertial Confinement laser Fusion (ICF) use so-called optical 'smoothing' methods for the laser beams interacting with the plasma corona in the ablating target, which is the outer target shell for the direct-drive scheme and the inner hohlraum wall for the indirect-drive scheme. Optical smoothing reduces the spatial and temporal coherence of the laser beams. It has the goal of mitigating and/or controlling the nonlinear processes related to laser-plasma interactions and hydrodynamic evolution of a target. So-called 'smoothed' laser beams have a smooth intensity distribution only on a coarse scale, while on a micro-scale, in the range of the laser wavelength, they exhibit a speckle structure. Such speckles, also called laser hot spots, generally all have similar sizes, along and across the laser propagation direction, which are defined by the focusing optics, and their peak intensity follows a well-known statistical distribution.

In both direct drive and indirect drive ICF schemes, laser beams cross each other, either by design of the beam configuration or because of partial reflections from the target surface. Besides the fact that laser beams can exchange energy due to resonances with plasma waves, known as Cross Beam Energy Transfer (CBET)[1, 2, 3, 4, 5, 6], such beams can have a complex substructure with important peak intensities in the speckles with values easily up to 10 times the average laser beam intensity. The ponderomotive force from the laser field on a plasma is defined as a gradient of the ponderomotive potential U. Using the definition of laser electric field $\vec{\mathcal{E}} = \frac{1}{2}[\vec{E}e^{-i\omega_0 t} + c.c.]$ with its envelope $\vec{E}$, obeying the time-dependent Helmholtz wave equation, the ponderomotive potential is defined as

$$U = e^2|\vec{E}|^2/(4m_e\omega_0^2). \tag{1}$$

where ω_0 is the laser frequency, e and m_e are the electron charge and mass, respectively. In the isothermal model of a plasma[7, 8, 9], usually satisfied for laser interactions with hot plasmas the low-frequency plasma response can be described by the continuity and momentum equations for cold ions

$$\frac{\partial n_i}{\partial t} + \nabla\cdot(n_i\vec{v}_i) = 0\ , \quad \frac{\partial \vec{v}_i}{\partial t} + (\vec{v}_i\cdot\nabla)\vec{v}_i = -\frac{Ze}{m_i}\nabla\phi \equiv -c_s^2\left(\frac{\nabla U}{T_e} + \nabla\log\frac{n_e}{n_0}\right) \tag{2}$$

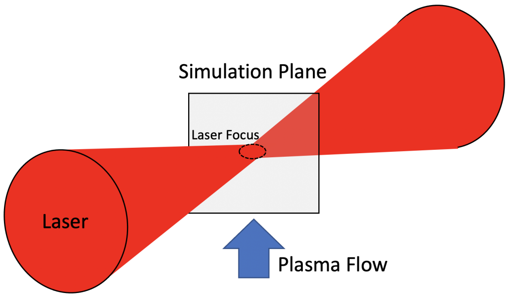

Figure 1: Schematic view of the interaction geometry: a large scale smoothed laser beam generates an imprint on the plasma in the beam focal region via its ponderomotive force. In numerical simulations, a two-dimensional (2D) domain is considered in the plane of the laser beam cross section at best focus where a super-sonic plasma flow is in the vertical direction (see an arrow).

where the electrostatic potential ϕ is replaced by the ponderomotive potential and the logarithm of electron density using the Boltzmann distribution for the electron density n_e, $n_e = n_0 \exp(e\phi/T_e - U/T_e)$ with n_0 describing the equilibrium density. In addition, $c_s \equiv \sqrt{ZT_e/m_i}$ stands for the ion sound speed, involving the electron temperature T_e, the ion charge Z and mass m_i. The ponderomotive potential can be given in practical units as $U/T_e \equiv 0.09 \, \langle I \rangle \lambda^2 (10^{15} \mathrm{W} \mu \mathrm{m}^2/\mathrm{cm}^2)/(T_e/keV)$, where $\langle I \rangle$ denotes the laser intensity and λ stands for the laser wavelength.
In a flowing plasma, the process of beam bending in the direction of the flow velocity has been examined in theory and experiments [10, 11, 12, 13]. The density perturbations resulting from the ponderomotive force of the laser are skewed by flow, which redirects the laser beam and by momentum conservation introduces a drag on the plasma flow slowing it down. The effect of beam bending is maximized producing the largest drag on the plasma flow when the flow velocity is close to the sound speed. The latter results in deceleration of the flow, and as the flow transitions from supersonic to subsonic velocity, conditions favourable to shock generation in the plasma can be reached. Our paper focuses on the formation of such shocks related to ponderomotively-driven density and velocity perturbations across the laser beam cross section.
Also spatio-temporal smoothing techniques, such as smoothing by spectral dispersion (SSD), commonly used at ICF facilities can lead to shock formation, as shown in this paper. Application of the SSD and RPP beams produces an enhancement of threshold conditions for shock generation.
One can estimate that a small change in the laser field averaged momentum flux due to angular deflection of the beam, characterized by the wave vector ratio, $k_\perp/k_0$, will affect the momentum of the flowing plasma. The change of the field momentum as $(k_\perp/k_0)\langle I \rangle/c$, with $\langle I \rangle = c\epsilon_0 \langle E^2 \rangle/2$ denoting the laser intensity, has to be compared with the change in the ion momentum flux $n_i m_i c_s^2 \delta M$ were the flow velocity is normalized to the speed of sound δM. Close to sonic flow with $v_i \approx c_s$, this yields an effective reduction of the flow velocity, namely $\delta M = (k_\perp/k_0)(\langle I \rangle/5 \times 10^{14} W/cm^2)(10^{20} cm^{-3}/n_i)(1keV/T_e)$. Deflecting the beam by an angle comparable with its angular aperture $k_\perp/k_0 \sim 1/(2F)$, corresponds to a flow reduction δM of ~ 0.125 for $\langle I \rangle \approx 10^{15} W/cm^2$, $n_i = 10^{20} cm^{-3}$, the beam optical f-number $F = 8$ and for the electron temperature $T_e = 1keV$.

2 Theory of laser beam deflection and shock formation by transverse plasma flow

The collective action of the speckles in the fine structure of smoothed laser beams with their intensities up to $10\times$ the average beam intensity can exert strong ponderomotive forces on the plasma, as described by Eqs. (2). Although local flow perturbations on the scale of individual speckles may be small, their cumulative effect over large beam as used in ICF will lead to shock formation[14, 15, 16], which can be intensified in regions of intersecting beams.
We investigate here how the small deflection of the electromagnetic momentum flux associated with beam bending induces an opposing change in momentum by decelerating the plasma flow.
By denoting $\vec{p}_\perp = (n_e/n_0)\vec{v}_\perp$ as the plasma fluid momentum density in the direction perpendicular to the laser propagation and $c_s = (ZT_e/m_i)^{1/2}$ as the sound speed, the isothermal fluid equations (2) one can consider a perturbative approach with respect to small velocity perturbations. Linearization around the background flow velocity, $\vec{v}_0$ in the x - y plane, $\vec{v}_\perp = \vec{v}_0 + \delta\vec{v}_\perp$ leads to the following set of equations [11]

$$(\partial_t + \vec{v}_0 \cdot \nabla_\perp) \ln \frac{n_e}{n_0} + \nabla_\perp \cdot \delta\vec{v}_\perp = 0, \quad (\partial_t + \vec{v}_0 \cdot \nabla_\perp) \delta\vec{v}_\perp + 2\hat{\nu}_{ia}\delta\vec{v}_\perp = -c_s^2 \nabla_\perp \left(\ln \frac{n_e}{n_0} + (1 + \hat{g}\ ) \frac{U}{T_e} \right) \tag{3}$$

where $\hat{\nu}_{ia}$ is a spatial convolution operator approximating Landau damping of ion acoustic perturbations. In Eqs. (3) the coupling between the laser and the plasma fluid is augmented with respect to Eqs. (2), by applying

an additional wave-number dependent spatial convolution operator $\hat{g}$ to the ponderomotive term, that accounts for both classical and non-local heat transport effects. This correction is obtained from a closure of the energy equation, see Ref. [17] and references therein. Equation (3) has to be solved by applying $\hat{g}$ in a Fourier space especially in the case when thermal effect dominate ponderomotive coupling, $\hat{g} > 1$. The Fourier transformed $\hat{g}$ reads[17] $g(k) = (1 + 50k\lambda_e)m_e\nu_{ei}^2/(7T_e k^2)$, where $k\lambda_e \propto T_e^2$ is the electron mean free path and $\nu_{ei} \propto T_e^{-3/2}$ is the electron-ion collision frequency. In the regime of classical thermal transport, $50k\lambda_e$ <1, the coefficient $g(k)$ scales with temperature as $g(k) \sim T_e^{-4}$; in the non-local, kinetic regime, $50k\lambda_e$ >1, it scales as $g(k) \propto T_e^{-2}$ where the spatial scale of the temperature inhomogeneity $1/k$ corresponds to $k \sim \pi/(F\lambda)$.
For the isothermal case, ignoring the correction $\hat{g}$, a stationary equilibrium can be reached in absence of flow by balancing the local density and the ponderomotive potential, namely $(n_e/n_0)_{v_\perp=0} \equiv \exp(-U/T_e)$.
Be aware that flow can considerably modify the response of the plasma fluid[18, 19, 10, 11, 20]. Time independent solution of Eqs. (3) yield in Fourier space[11] $[\ln n_e/n_0]_{k_\perp} = [\ln(n_e/n_0)_{v_\perp=0}]_{k_\perp}[1-(k_y/k_\perp)\mathcal{M}(k_y\mathcal{M}/k_\perp-2i\hat{\nu})]^{-1}$ in which the background flow $\vec{v}_0$ is chosen along the y-axis, the Mach number $\mathcal{M} = v_y/c_s$ and the normalized damping operator $\hat{\nu} = \nu_{ia}/(kc_s)$. The density perturbation shows a skewed profile due to the flow compared to ρ_0 in the stationary plasma and the ponderomotive potential U of a single laser speckle. This asymmetry in density perturbations averaged over speckles of the randomized laser beam leads to beam bending. In the small angle approximation the beam bending can be quantified by the averaged angular deflection rate [11]

$$\frac{\partial\langle\theta\rangle}{\partial z} = \frac{\partial}{\partial z}\left\langle \vec{k}_\perp/k_0 \right\rangle_k \cdot \vec{e}_v = -\frac{\langle\nabla_\perp\delta n\rangle_r}{2n_c}\cdot\vec{e}_v = \frac{2\beta}{F\lambda}\frac{\langle n\rangle_r}{n_c}\frac{\langle U\rangle_r}{T_e} f(\mathcal{M},\hat{\nu}) \tag{4}$$

with the unit vector $\vec{e}_v$ pointing in the flow direction and where the small density perturbation $\delta n/n_0 = (n_e - n_0)/n_0 \simeq \ln n_e/n_0$. The averages $\langle\rangle_{k,r}$ in the two dimensional Fourier (k)- or configuration (r)- space of any function $h(\vec{q})$, are defined as follows $\langle h\rangle_q(z) = \int |E(\vec{q},z)|^2 h(\vec{q})d^2q/(\int |E(\vec{q},z)|^2 d^2q)$ with q standing for either $k_\perp$ or $\vec{r}_\perp$. The rate of beam deflection Eq. (4) and the averaging involve the electric field amplitude $\vec{E}$ which is determined by solving the paraxial wave equation for the laser field.
The right-hand-side (rhs) of Eq. (4) has been derived in Ref. [15], see in particular Eq. (157) there, for the case of a randomized laser field generated by introducing random phase plates in the focusing optics, which is characterized by the averaged ponderomotive potential $\langle U\rangle$ and the speckle correlation length given by $\ell_{\rm sp} = F\lambda/\beta$ with $\beta = 64/45$, and with F and λ denoting the focusing F-number and the laser wave length, respectively. The function $f()$ used in the rhs of Eq. (4) results from an integral over the angle between the flow and the wave vector of the ponderomotively driven ion acoustic waves[21]. It depends essentially on the regime of the plasma flow component across the laser beam cross section, in terms of the Mach number M, and the ion acoustic damping $\hat{\nu}$ (which is wave number-dependent, typically $\propto k$). There is no effective beam deflection for subsonic flow, except in the close vicinity of sonic flow with a resonant transfer into another beam, however only over a short range until the flow is no longer orthogonal to the beam propagation.
The beam deflection occurs for a super-sonic flow and for the case of negligible damping with respect to $\mathcal{M}^2 - 1$, the function $f(\mathcal{M},\hat{\nu})$ simplifies into the expression $\hat{f}(\mathcal{M}) = 1/(2\mathcal{M}\sqrt{\mathcal{M}^2-1})$.
Note that for regimes in which thermal effects modify the laser-plasma coupling via the ponderomotive potential with the $1 + \hat{g}$ correction (see above), the rhs of Eq. (4) is modified: additional terms coming from $g(k)$ have to be taken into account via the integration over the speckle correlation function[16].
In order to determine the cumulative action of the ponderomotive force from numerous speckles it is useful to introduce a scale separation between the mean values and the fluctuation of the fluid quantities, namely for the momentum $\vec{p}_\perp = \langle\vec{p}_\perp\rangle + \delta\vec{p}_\perp$ in Eqs. (3). This results[11, 16] in reduction of the averaged fluid momentum as a function of time, due to the collective action of speckles. The slowing down of the plasma flow can be described in terms of a drag force by ignoring the averages of fluctuating terms except in the last term on the rhs of Eq. (3). This leads to equations for the averages $\langle\vec{p}_\perp\rangle$ and $\langle n\rangle$,

$$\partial_t\langle\vec{p}_\perp\rangle + \nabla_\perp\cdot(\langle\vec{p}_\perp\rangle\langle\vec{v}_\perp\rangle) = -\alpha\,\langle\vec{p}_\perp\rangle - c_s^2\nabla_\perp\left(\ln\langle n/n_0\rangle + \frac{\langle U\rangle}{T_e}\right) \text{ with } \alpha = 4\beta\frac{c_s}{F\lambda}\left(\frac{\langle U\rangle}{T_e}\right)^2\frac{f(\mathcal{M},\nu_{ia})}{\mathcal{M}} \tag{5}$$

where $\alpha \propto \partial_z\langle\theta\rangle$ is the drag coefficient. We assume an idealized laser beam whose spatial envelope is a slab, varying in the y-direction, and assume flow in positive y-direction with the (local) Mach number $\mathcal{M} \equiv \langle v_y\rangle/c_s >$ 1 at $y = 0$. The density profile is initially unperturbed, but the ponderomotive force inside the speckle pattern acts on the plasma. The drag effect, as described above, leads to the deceleration of supersonic flow, transitioning it from the supersonic to subsonic flow regime. The latter gives rise to the shock formation. Combining steady state flow, Eq. (5), and the continuity equation, yields the relation

$$(\langle\vec{v}_\perp\rangle\cdot\nabla_\perp)\,\langle\vec{v}_\perp\rangle + c_s^2\nabla_\perp\ln\langle n/n_0\rangle + \alpha\,\langle\vec{v}_\perp\rangle = -c_s^2\,\nabla_\perp\langle U\rangle/T_e \tag{6}$$

where the source term can be neglected because it involves taking a derivative of the averaged ponderomotive potential which has no speckle structure. For the isothermal case without the correction for thermal transport,

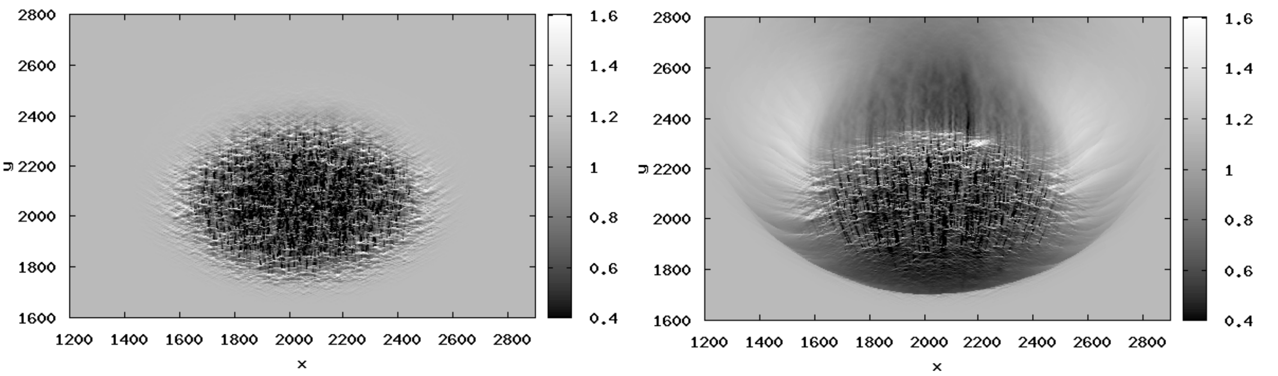

Figure 2: Cross sections from a simulation showing the plasma flow v_y/c_s (see bar with gray scale)in x and y, in units of the laser wave length λ. Left: at early time, showing laser speckle imprint. Right: late time with already developed shock front departing from the laser speckle pattern. Incoming flow at M =1.2 (from below).

the homogeneous part of Eq. (6) can be rewritten in terms of the Mach number $\mathcal{M}$ yielding together with Eq. (4) and $\nabla_\perp \to \partial_y$,

$$\frac{d}{dy}\left(\mathcal{M}+\frac{1}{\mathcal{M}}\right) = -\frac{2\beta}{F\lambda}\left(\frac{\langle U\rangle}{T_e}\right)^2 \frac{1}{\mathcal{M}^2\sqrt{\mathcal{M}^2-1}} \quad \text{yielding} \quad \frac{y_{sonic}}{y_p} = \frac{1}{2\beta}\int_1^M (\mathcal{M}^2-1)^{3/2} d\mathcal{M} \tag{7}$$

which determines the position y_{sonic}, at which the incoming super-sonic flow is decelerated to sonic velocity. The integral in (7) is simply a function of the Mach number M of the incoming flow. The position y_{sonic} depends on the value of M, and it defines the plasma penetration depth within the laser beam necessary for the onset of shock formation; y_{sonic} scales with $y_p = F\lambda/(\frac{\langle U\rangle}{T_e})^2$, i.e. with the speckle correlation length, $F\lambda/\beta$ and is inversely proportional to the square of the ponderomotive potential.
For regimes in which thermal effects dominate the laser-plasma coupling, $\hat{g} > 1$, the y_{sonic} length will be modified with respect to Eq. (7).

3 Shock formation in numerical simulations with optically smoothed laser beams

We have performed numerical simulations with a conservative hydrodynamic scheme, based on the Clawpack package [22, 23] and adapted to a hot isothermal plasma[24] in two dimensions (2D). The ponderomotive potential of the laser beam with speckle structure, taken in a single cross section close to the laser beam focus was applied as source term in Eq. (2). For these simulations an initially homogeneous electron density of n_e =0.1n_c is assumed where n_c is the critical density. The simulations are performed in dimensionless units, where spatial coordinates are normalized to the laser wavelength λ and time is measured in λ/c_s. The ion sound speed, c_s, reads in practical units as $\sim 0.3\mu$m/ps $\times\sqrt{ZT(keV)/A}$.
For the smoothed laser beams we have used the focusing F-number F =8. The spatial domain was resolved with 4096x4096 mesh points. For the typical laser wave length of λ =0.351μm this corresponds to a spatial resolution of $dx = dy$ =0.483μm for a domain size defined by $L_x = L_y$ =1.977mm.
The spatial incoherence of laser beams is introduced using the top hat model for the Random Phase Plates (RPP)[25]. For the beam intensity distribution within the $x-y$-plane inside the plasma, the corresponding

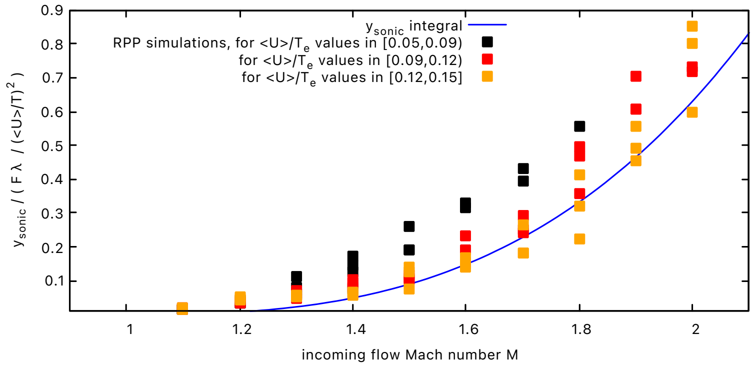

Figure 3: Comparison between the scaled position y_{sonic} from simulations (data points) and from Eq. (7).

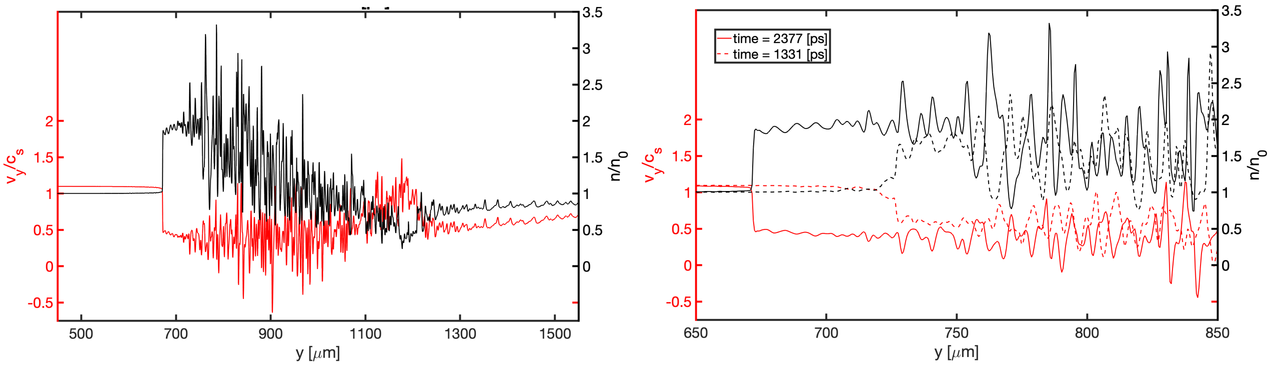

Figure 4: Density and flow profiles, n_1/n_0 (in black) and v_y/c_s (red colour), respectively, along the y-axis across the beam propagation and along the incoming supersonic flow, here M =1.2 taken at the central cut of the laser beam cross section. Left: profiles across the entire laser beam speckle pattern taken at late time, t =2.38ns, right: profiles zoomed around the shock emerging from the speckle pattern, $y \sim$700µm, taken at two instants, t =1.33ns and later t =2.38ns. Spatial units in µm for $\lambda = 0.351\mu m$.

near field configuration at the focusing lense is composed of elements with a random phase $\phi(\vec{k})$, i.e. 0 or $\pi/2$ (RPP), and a constant amplitude $|E(\vec{k})|$ for $|\vec{k}| \leq k_0/(1+4F^2)^{1/2}$ (and 0 outside) with $k_0 = 2\pi/\lambda$ for the laser wavenumber. The laser electric field in the interaction zone, where the plasma is situated, is computed via the Fourier transform of $E(\vec{k}_\perp)\exp(ik_\perp^2 z/2k_0)$. The cross-section of the speckle patterns produced by such disk-shaped RPP beams are seen in the ponderomotively induced flow velocity (v_y/c_s) perturbations in Fig. 2, left subplot. In the same figure, right subplot, a smooth shock front emerges from the region dominated by the beam speckle pattern.

In an early stage of shock formation, the position y_{sonic} at which the flow transitions from the super- $(y < y_{sonic})$ to the sub-sonic $(y > y_{sonic})$ velocity appears inside and close to the edge of the laser beam cross section with a speckle structure. This position y_{sonic} has been determined from a set of simulations with RPP-smoothed laser beams by varying the amplitude of $\langle U\rangle/T_e$ and the incoming flow Mach number M. The comparison with the theory developed in the preceding section, Eq. (7), blue line, shows good agreement between simulations and the model, and confirms the scaling with $y_p = F\lambda/(\frac{\langle U\rangle}{T_e})^2$. Different colours distinguish data points with different ponderomotive coupling strength, see legend.

The shock front that emerges from the beam cross section, as seen in Fig. 2, right subplot, can be quantified by determining the density and flow speed jumps, n_1/n_0, and v_y/c_s, respectively.

At the major laser laser facilities dedicated to ICF and to laser-plasma interaction experiments, spatio-temporal smoothing techniques are used, in particular Smoothing by Spectral Dispersion (SSD)[26, 27] such as at the US National Ignition Facility (NIF), the Omega laser at the U. of Rochester and the French Laser MégaJoule (LMJ). SSD makes use of a bandwidth in the laser pulse in combination with a grating that leads to the motion of speckles [28], which is in contrast to the steady state speckle pattern for the case of RPP. While SSD can be implemented both transversely and longitudinally[29], we restrict ourselves here to transverse SSD as is implemented on the NIF.

In a first stage of SSD, sinusoidal phase modulations to the pulse introduce bandwidth before the beam passes through a dispersion grating tilting the pulse front. The electric field at the lens can be written as $\mathbf{E}(y,t) = \frac{1}{2}\mathbf{E}_0(y,t)\exp\{i[\omega_0 t + \delta_m \sin(\omega_m t + 2\pi N_{cc} y/w_y) + \phi_0]\} + c.c.$ where ω_0 is the central laser frequency, ϕ_0 the initial phase, ω_m the modulation frequency, δ_m the modulation depth, N_{cc} is the number of colour cycles and w_y is the beam width in y direction. The resulting total bandwidth of the laser pulse $\Delta\omega \approx 2\delta_m\omega_m$ which is still small relative to the ω_0. The value of δ_m has to be multiplied by 3 for frequency-tripled laser pulses (λ =.351µm).

In our simulations applying the spatio-temporal smoothing technique SSD, we observe very similar evolution of the shock front departing from the laser beam cross section, as seen for the case of RPP. Please consult Ref. [21] for details that distinguish RPP and SSD as far as the y_{sonic} position is concerned. The results shown in Fig. 4 correspond even to the case of SSD with $3\times\delta_m$ =1.8 and ω_m =17GHz. They are in qualitative agreement with RPP simulations but for the same parameters M and $\langle U\rangle/T_e$, SSD tends to produce stronger shocks, as shown in Fig. 5, which summarizes results from a set of RPP and SSD simulations by varying M and $\langle U\rangle/T_e$, left subplot.

4 Shock strength and shock speed: simulations vs. theory

The results of our set of simulations for cases with pure spatial and with spatio-temporal smoothing, RPP and SSD, respectively, are shown in Fig. 5, both for the shock strength in terms of the density jump across the shock

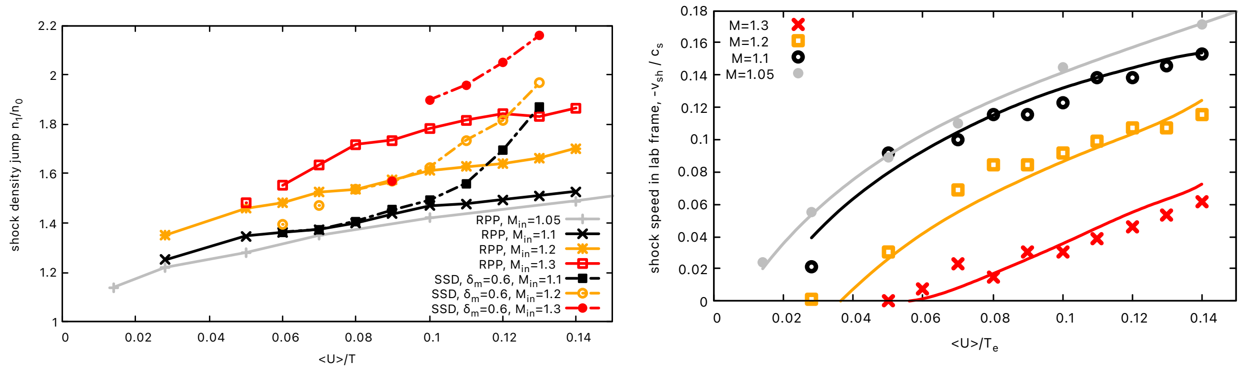

Figure 5: Left: Shock density jump, for both RPP and SSD cases, right: RPP only, speed of the shock front after outbreak from the beam cross section, dots for simulations, lines from Eq. (8), both as a function of the normalized ponderomotive potential $\langle U\rangle/T_e$ for different values Mach number of the incoming flow, M.

front, n_1/n_0, and the shock speed in the laboratory frame $v_{\rm sh}/c_s$. Both sets of values are determined from the shock front evolution as shown in Fig. 4. The speed of the emerging shock depends on the ponderomotive force and can be determined by integrating Eq. (6) from the upstream region of unperturbed plasma over the shock front into the region of the speckle pattern. It yields for the cases of RPP, without temporal smoothing (i.e. not for SSD), the following relation between the density jump n_1/n_0, the ponderomotive potential $\langle U\rangle/T_e$, Mach number of the incoming flow, and the shock speed in the laboratory frame,

$$\left(M - \frac{v_{\rm sh}}{c_s}\right)^2 = 2\frac{\langle U\rangle/T_e + \ln(n_1/n_0)}{1-(n_1/n_0)^{-2}}. \tag{8}$$

for the derivation of which we have used the continuity equation in the shock frame. The data points in the right subplot of Fig. 5 correspond to the values directly deduced from the simulations, by inspecting the advancing shock front for each case. The lines in Fig. 5 have been deduced from our model, Eq. (8), that takes into account the ponderomotive action of the laser beam on the plasma flow. For the evaluation of expression Eq. (8) we have used the values for the density jumps (reported in the left sublplot of Fig. 5) from our simulations in order to determine $-v_{\rm sh}/c_s$, as shown in the lines of the right subplot of Fig. 5.
Assuming that a smooth shock front develops, cf. Fig. 2, and can propagate outside the beam cross section, the shocks should obey the Rankine-Hugoniot relations, resulting from continuity, momentum, and energy balance in the frame of the shock, see e.g. [30].
For an isothermal plasma, as considered in our simulations, we disregard the internal energy relations on both sides of the shock. For this case, the sound speed is the same on both sides, such that the simplified Rankine-Hugoniot relations result in $n_1/n_0 = \mathcal{M}_0^2 = \mathcal{M}_1^{-2}$ together with $\mathcal{M}_0\mathcal{M}_1 = 1$, in the shock frame (!), with '0' for upstream, unperturbed, and '1' and dowstream. The resulting density jump is then essentially a function of the Mach numbers, relating $\mathcal{M}_1^2 = M^2$ to the incoming flow, and to the shock speed $v_{\rm sh}$ in the laboratory frame as $-v_{sh}/c_s = \sqrt{n_1/n_0} - M$. This implies that the formation of a shock propagating against the incident flow ($-v_{sh} > 0$) can only occur for a sufficiently high density jump, namely $n_1/n_0 > M^2$; consequently for M =1.05, 1.1, 1.2, and 1.3 this means that shocks should not be able to leave the laser beam cross-section and propagate freely unless n_1/n_0 >1.10, 1.21, 1.44, and 1.69, respectively. This explains also why the simulation data shown in Fig. 8 for M =1.3 are incomplete for smaller $\langle U\rangle/T$ values. Consequently, the data points for M =1.3 and $\langle U\rangle/T_e$ <0.08 have large uncertainty associated with their values. At the same time, as shown in Fig. 5, the strength of the shock in terms of the jump conditions increases with M, as a consequence of the condition $n_1/n_0 > M^2$, and increases with the cumulative action of the ponderomotive force in the beam speckles, $\propto \langle U\rangle/T_e$.
It is important to note that the time required to observe a shock emerging out of the laser beam cross-section can be very long, beyond the run time of our simulations, because of the low shock speed. This trend of lower shock speeds, but at the same time higher shock strengths, increases with the incoming Mach number as seen in Fig. 8.

5 Conclusion

Optically smoothed laser beam with speckle structure can lead to the formation of macroscopic shocks emerging from the beam cross section in presence of incoming flow that has a supersonic speed perpendicular to the laser beam propagation axis. The shock that forms in the direction against the incoming supersonic flow results from the cumulative action due to the ponderomotive force from the laser speckle ensemble of smoothed beam. The characteristic distance of plasma penetration across the randomized laser beam required for the flow to

slow down to subsonic velocity and form a shock, given by Eq. (7), is an indicator for the likelihood of shock generation.
The emergence of such shocks can occur when smoothed laser beams propagate through hot expanding plasmas with at least slightly supersonic flow, and when such beams are subject to bending together with the resulting momentum change induced by the redirected laser light. Such scenarios are likely to occur in laser generated plasmas in the context of laser-driven ICF, both for the indirect- and the direct-drive schemes.
Based on our simulations with RPP beams for the average laser intensity $I = 2 \times 10^{15}$ W/cm^2, $F\lambda$=$1\mu m$ and electron temperature T_e=2 keV, resulting in the normalized ponderomotive potential $\langle U\rangle/T_e \approx 0.011$, and an incoming flow velocity corresponding to $1.05 \leq M_{in} \leq 1.2$, we find that the distance y_{sonic} to shock formation within the laser is approximately 0.05-0.1 $F\lambda/(\langle U\rangle/T_e)^2$ (see Fig. 3), i.e. approximately 400-810μm. The estimated time to observe such a shock, would be roughly 1.3-2.7 ns. Hence, within the square cross section of 400μm$\times$ 400μm or 810μm $\times$ 810μm of the laser beam with an average intensity $I = 2 \times 10^{15}$ W/cm^2 will require the energy of 9kJ or 36kJ, respectively.
In the current work, we have restricted ourselves to the case of an isothermal plasma without any effects from local or non-local heat transport and collisional plasma heating. The latter may play a role in cases of non-uniform heating and/or transport mechanisms with electron mean free paths comparable or beyond the speckle size. This may be of importance for plasma electron temperatures below 1keV. Currently we study the shock generations taking into account such processes, both by considering the enhancement of the speckle structure and its ponderomotive force following adequate models[17] and by performing numerical simulations taking into account collisional absorption and thermal transport.

Acknowledgments

SH acknowledges the access granted to the French HPC resources of IDRIS under the allocations A0100500573 and AD010500573R1 by GENCI, as well as the support by the CPHT computer team. AM and WR acknowledge support from the Digital Research Alliance of Canada and support from the U.S. Department of Energy Contract number: DE-NA0004144. This work was performed under the auspices of the U.S. Department of Energy by Lawrence Livermore National Laboratory under Contract DE-AC52-07NA27344 and by LLNL's WPD, ICF Program's Academic Collaboration Teams's University Program (ACT-UP) under Subcontract No. B645970.

6 References

[1] W. L. Kruer, S. C. Wilks, B. B. Afeyan, and R. K. Kirkwood, "Energy transfer between crossing laser beams," *Phys. Plasmas*, vol. 3, no. 1, pp. 382–385, 1996.

[2] R. K. Kirkwood, B. B. Afeyan, W. L. Kruer, B. J. MacGowan, J. D. Moody, D. S. Montgomery, D. M. Pennington, T. L. Weiland, and S. C. Wilks, "Observation of energy transfer between frequency-mismatched laser beams in a large-scale plasma," *Phys. Rev. Lett.*, vol. 76, pp. 2065–2068, Mar 1996.

[3] V. V. Eliseev, W. Rozmus, V. T. Tikhonchuk, and C. E. Capjack, "Interaction of crossed laser beams with plasmas," *Physics of Plasmas*, vol. 3, pp. 2215–2217, 06 1996.

[4] P. Michel, L. Divol, E. A. Williams, S. Weber, C. A. Thomas, D. A. Callahan, S. W. Haan, J. D. Salmonson, S. Dixit, D. E. Hinkel, M. J. Edwards, B. J. MacGowan, J. D. Lindl, S. H. Glenzer, and L. J. Suter, "Tuning the implosion symmetry of icf targets via controlled crossed-beam energy transfer," *Phys. Rev. Lett.*, vol. 102, p. 025004, 2009.

[5] P. Michel, L. Divol, E. A. Williams, C. A. Thomas, D. A. Callahan, S. Weber, S. W. Haan, J. D. Salmonson, N. B. Meezan, O. L. Landen, S. Dixit, D. E. Hinkel, M. J. Edwards, B. J. MacGowan, J. D. Lindl, S. H. Glenzer, and L. J. Suter, "Energy transfer between laser beams crossing in ignition hohlraums," *Phys. Plasmas*, vol. 16, no. 4, p. 042702, 2009.

[6] A. Colaïtis, S. Hüller, D. Pesme, G. Duchateau, and V. T. Tikhonchuk, "Crossed beam energy transfer: Assessment of the paraxial complex geometrical optics approach versus a time-dependent paraxial method to describe experimental results," *Physics of Plasmas*, vol. 23, no. 3, p. 032118, 2016.

[7] J. Candy, W. Rozmus, and V. T. Tikhonchuk, "Nonlinear ion waves driven by the periodic ponderomotive force," *Phys. Rev. Lett.*, vol. 65, pp. 1889–1892, Oct 1990.

[8] S. Hüller, "Stimulated brillouin scattering off nonlinear ion acoustic waves," *Physics of Fluids B: Plasma Physics*, vol. 3, no. 12, pp. 3317–3330, 1991.

[9] H. A. Rose, "Saturation of stimulated brillouin scatter by self-consistent flow profile modification in laser hot spots," *Physics of Plasmas*, vol. 4, no. 2, pp. 437–446, 1997.

[10] D. E. Hinkel, E. A. Williams, and C. H. Still, "Laser beam deflection induced by transverse plasma flow," *Phys. Rev. Lett.*, vol. 77, pp. 1298–1301, Aug 1996.

[11] H. A. Rose, "Laser beam deflection by flow and nonlinear self-focusing," *Physics of Plasmas*, vol. 3, no. 5, pp. 1709–1727, 1996.

[12] J. D. Moody, B. J. MacGowan, D. E. Hinkel, W. L. Kruer, E. A. Williams, K. Estabrook, R. L. Berger, R. K. Kirkwood, D. S. Montgomery, and T. D. Shepard, "First optical observation of intensity dependent laser beam deflection in a flowing plasma," *Phys. Rev. Lett.*, vol. 77, pp. 1294–1297, Aug 1996.

[13] B. Bezzerides, "Intrinsic bending of a laser beam in a flowing plasma," *Physics of Plasmas*, vol. 5, no. 7, pp. 2712–2720, 1998.

[14] H. A. Rose and S. Ghosal, "Effect of smoothing by spectral dispersion on flow induced laser beam deflection: The random phase modulation scheme," *Physics of Plasmas*, vol. 5, no. 3, pp. 775–781, 1998.

[15] S. Ghosal and H. A. Rose, "Two-dimensional plasma flow past a laser beam," *Physics of Plasmas*, vol. 4, no. 7, pp. 2376–2396, 1997.

[16] S. Ghosal and H. A. Rose, "Effect of induced spatial incoherence on flow induced laser beam deflection: Analytic theory," *Physics of Plasmas*, vol. 4, no. 12, pp. 4189–4191, 1997.

[17] H. A. Rose and D. F. DuBois, "Modification of stimulated Brillouin, saturated Raman scattering and strong Langmuir turbulence by nonlocal heat transport," *Physics of Fluids B: Plasma Physics*, vol. 4, pp. 1394–1396, 06 1992.

[18] R. W. Short, R. Bingham, and E. A. Williams *Phys. Fluids*, vol. 25, no. 12, pp. 2302–2303, 1982.

[19] A. J. Schmitt, "The effects of plasma flow on thermal and ponderomotive light filamentation," *Physics of Fluids B*, vol. 1, no. 6, pp. 1287–1294, 1989.

[20] C. Ruyer, P. Loiseau, G. Riazuelo, R. Riquier, A. Debayle, P. E. Masson-Laborde, and O. Morice, "Accounting for speckle-scale beam bending in classical ray tracing schemes for propagating realistic pulses in indirect drive ignition conditions," *Matter and Radiation at Extremes*, vol. 8, no. 2, p. 025901, 2023.

[21] J. D. Ludwig, S. Hüller, H. A. Rose, C. Bruulsema, W. Farmer, P. Michel, A. L. Milder, G. F. Swadling, and W. Rozmus, "Shock formation in flowing plasmas by temporally and spatially smoothed laser beams," *Physics of Plasmas*, vol. 31, no. 3, p. 032103, 2024.

[22] R. J. L. Vecque, "Wave propagation algorithms for multidimensional hyperbolic systems," *J. Comp. Phys.*, vol. 131, no. CP965603, pp. 327–353, 1997.

[23] R. J. LeVeque, *Numerical Methods for Conservation Laws.* Birkhauser Basel, 1992.

[24] S. Hüller, P. E. Masson-Laborde, D. Pesme, M. Casanova, F. Detering, and A. Maximov, "Harmonic decomposition to describe the nonlinear evolution of stimulated brillouin scattering," *Phys. Plasmas*, vol. 13, no. 2, p. 022703, 2006.

[25] H. A. Rose and D. F. DuBois, "Statistical properties of hot spots produced by a random phase plate," *Phys. Fluids B*, vol. 5, pp. 590–596, 1993.

[26] S. Skupsky, R. W. Short, T. Kessler, R. S. Craxton, S. Letzring, and J. M. Soures, "Improved laser-beam uniformity using the angular dispersion of frequency-modulated light," *Journal of Applied Physics*, vol. 66, no. 8, pp. 3456–3462, 1989.

[27] T. R. Boehly, V. N. Goncharov, O. Gotchev, J. P. Knauer, D. D. Meyerhofer, D. Oron, S. P. Regan, Y. Srebro, W. Seka, D. Shvarts, S. Skupsky, and V. A. Smalyuk, "Optical and plasma smoothing of laser imprinting in targets driven by lasers with SSD bandwidths up to 1 THz," *Physics of Plasmas*, vol. 8, pp. 2331–2337, 05 2001.

[28] F. Walraet, G. Bonnaud, and G. Riazuelo, "Velocities of speckles in a smoothed laser beam propagating in a plasma," *Physics of Plasmas*, vol. 8, no. 11, pp. 4717–4720, 2001.

[29] A. Fusaro, R. Collin, G. Riazuelo, P. Loiseau, O. Thauvin, and D. Penninckx, "On the improvement of smoothing by spectral dispersion efficiency for laser–plasma interaction," *Physics of Plasmas*, vol. 31, p. 012110, 01 2024.

[30] J. Spurk and N. Aksel, *Fluid Mechanics.* Springer International Publishing, 2019.